Journal of Materials Chemistry C

Accepted Manuscript

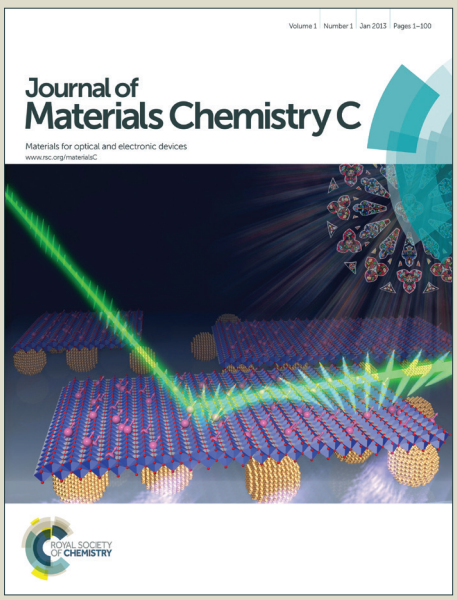

ROYAL SOCIETY OF CHEMISTRY

www.rsc.org/materialsC

Journal of Materials Chemistry C

Journal of Materials Chemistry C

Dynamic Article Links►

Cite this: DOI: 10.1039/coxx00000x

PAPER

www.rsc.org/xxxxxx

Molecular order of air-stable p-type Organic Thin-Film Transistors by tuning the extension of the π-conjugated core: the cases of Indolo[3,2-*b*]carbazole and Triindole semiconductors

Marta Reig,[a] Joaquim Puigdollers[b] and Dolores Velasco*[a]

Received (in XXX, XXX) XthXXXXXXXXX 20XX, Accepted Xth XXXXXXXXX 20XX
DOI: 10.1039/b000000x

Charge transport in organic devices depends strongly on the molecular order and morphology of the organic semiconductor thin films. In the design of new organic semiconductors, the selection of the appropriate core plays a key role in the molecular packing and charge transport characteristics of the organic device. Four derivatives of carbazole that mainly differ in the extension of the π-conjugated core, including indolo[3,2-*b*]carbazole and triindole derivatives, exhibited hole mobilities ranging from 10^{-5} to 10^{-2} $cm^2V^{-1}s^{-1}$ as active layers in Organic Thin-Film Transistors (OTFTs). X-ray analysis of single crystals and evaporated thin films gave insights into the molecular packing of the compounds that justified their OTFTs characteristics.

Introduction

After intensive research efforts, p-type OTFTs have successfully reached hole mobilities comparable to the obtained with amorphous silicon. OTFTs performance has experienced an impressive progress in the recent years due to the processing of new materials, device geometries and morphology control. However, the properties of organic semiconductors still determine the OTFTs device performance. In view of that, when designing new suitable organic compounds for molecular electronics, the selection of an appropriate core structure is one significant aspect to take into account[1], since it could modulate the optical and electronic properties and even, determine the stability and durability under ambient conditions of the fabricated devices. One strategy to achieve materials with high air stability is to work with compounds exhibiting low-lying High Occupied Molecular Orbital (HOMO) levels in order to obtain stable compounds against oxidative doping by atmospheric oxygen.

The search of high mobility organic semiconductors has yielded pentacene as one of the most promising materials reaching high hole mobilities of 3 $cm^2V^{-1}s^{-1}$for vacuum deposited OTFTs.[1b,2] Nevertheless, pentacene based devices present several drawbacks for practical applications due to a lack of air stability and fast device degradation.[3]

Carbazole derivatives have been widely studied as hole-transporting semiconductors due to its electron-donating capabilities.[4] In addition, they are recognised as reasonable stable compounds against oxidative doping by atmospheric oxygen. The carbazole unit presents a series of advantages in front of other conventional organic semiconductors such as its low cost, easy availability and its high stability in front of environmental conditions.

In this work we deal with the study of 9-methyl-9*H*-carbazole **1**, 9,9'-dimethyl-9*H*,9*H*'-[3,3']bicarbazole **2**, 5,11-dimethyl-indolo[3,2-*b*]carbazole **3** and *N*-trimethyltriindole **4** (Figure 1) as active organic semiconductor layers in OTFTs. Within this series, the extension of the π-conjugated core was progressively varied, leading to improved OTFTs performances of 10^{-2} $cm^2V^{-1}s^{-1}$.

Indolo[3,2-*b*]carbazole and triindole show extended π systems in which two or three carbazole units, respectively, share an aromatic ring. Indolo[3,2-*b*]carbazole and triindole unit present a planar structure with two or three N-H units, respectively, which allows easy introduction of alkyl chains in order to increase the solubility of the systems and to promote the molecular order of the materials during the deposition process. Both heterocycles display large energy band gaps and low-lying HOMO energy

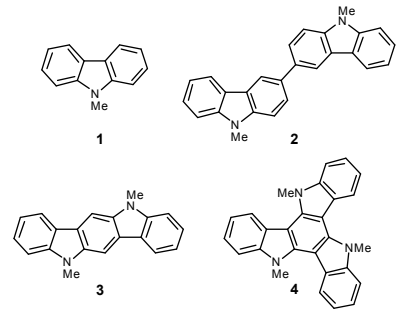

Fig. 1 Molecular structure of carbazole based derivatives **1**-**4**.

levels. In the last years, indolocarbazole has received special attention as a building block in the field of organic electronics and recent studies have shown the great potential of indolo[3,2-*b*]carbazole derivatives to be used in OTFTs.[5] The triindole core presents a larger molecular structure than the indolocarbazole one. Accordingly, higher molecular order could be expected from it and therefore, better charge carrier transport. To the best of our knowledge, there are still no studies about the application of triindole derivatives in OTFTs. Recently, triindole derivatives have been described as suitable organic materials in Organic Solar Cells (OSCs)[6] and OLEDs.[7] Charge transport properties of liquid crystal based triindole derivatives[8] and of triindole **4** have been reported by the space-charge-limited-current method (SCLC), yielding values of hole mobilities for the later ranging from ~ 1 ×10^{-4} to ~ 1 ×10^{-3} $cm^2V^{-1}s^{-1}$.[6b] The easy preparation, high thermal stability, π-stacking capability, high carrier mobilities and optoelectronic properties of such molecules make indolocarbazole and triindole based materials very promising organic semiconductors for optoelectronic applications.

Here we report not only the OTFT performance of carbazole containing compounds **1**-**4**, but also the determination of the molecular packing in the organic semiconductor layer of the devices by means of X-ray diffraction (XRD) studies. Therefore, the aim of this work is to determine the correlation of the device performance with the molecular order in the semiconducting thin films in function of the π-conjugated core design of the organic semiconductors.

Results and discussion

Synthesis and physical properties

Compound **2** was synthesized by oxidative dimerization of 9-methyl-9*H*-carbazole with $FeCl_3$ in anhydrous chloroform following a procedure reported in the literature.[9] Indolo[3,2-*b*]carbazole was synthesized by condensation of 1,4-cyclohexanodione with phenylhydrazine followed by double Fischer indolization.[10] Triazatruxene was synthesized by cyclocondensation of 2-oxindole.[11] *N*-methyl derivatives **1**, **3** and **4** of the corresponding 9*H*-carbazole, indolo[3,2-*b*]carbazole and triazatruxene were obtained by methylation under standard conditions in high yields. Compounds **1**-**4** were fully characterized by ^{1}H-NMR, ^{13}C-NMR and MS.

Indolocarbazole **3** and triindole **4** exhibited high thermal stability by thermal gravimetric analysis (TGA) showing the onset decomposition at 384 ºC and 461 ºC, respectively.

Compounds **1**-**4** showed one oxidation process by cyclic voltammetry, whereas no reduction processes were observed for all of them. Table 1 collects the electrochemical characteristics, the HOMO energy level estimated from cyclic voltammetry and the energy band gap estimated from UV-visible (Absorption spectra and cyclic voltammograms can be found in the ESI, Fig. S1-S2†). In this series of carbazole-based compounds, increasing the conjugation of the system, HOMO levels are slightly destabilized from -5.81 eV for carbazole **1** to -5.10 eV corresponding to triindole derivative **4** (Figure 3). The relative low-lying HOMO levels and high HOMO-LUMO gaps (~3 eV) of these compounds are indicative of their potential hole transporting properties. Moreover, the energy levels found for the organic semiconductors **1**-**4** are perfectly suitable to Au electrode work function (-5.1 eV) as it is displayed in Figure 2, being triindole **4** HOMO level of -5.1 eV, indicating a potential efficient charge injection in the OTFT device performance.

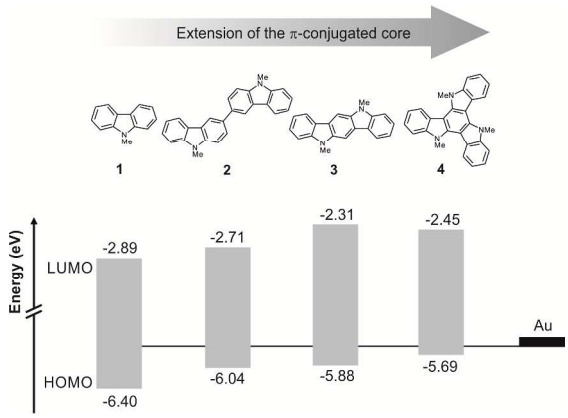

Fig. 2 Energy levels (HOMO-LUMO) of materials **1**-**4** measured by cyclic voltammetry. Gold is showed for comparison.

Organic Thin-Film Transistors

Charge carrier mobilities were measured by using the organic materials **1**-**4** as vacuum-deposited active layers in standard bottom gate-top contact OTFTs.

Fabrication of OTFTs with compound **1** as the organic semiconductor layer was not successful due to its low sublimation temperature (40ºC at 10^{-6} mbar under the experimental conditions during the deposition process). **2** based devices fabricated with 50 nm thick SiO_2 dielectric presented a bad yield and reproducibility: only 17% of the devices fabricated with polystyrene (PS) treated substrates presented OTFT characteristics, with a maximum hole mobility around 2 × 10^{-5} $cm^2V^{-1}s^{-1}$ and a threshold voltage of -16.0 V (Table 1).

Table 1 Optical and electrochemical properties for compounds **1**-**4** and OTFTs characteristics of devices based on **1**-**4** carbazole derivatives with polystyrene treated c-Si/SiO_2 substrates.

compound	λ_{abs} (ε) [a] nm ($M^{-1}cm^{-1}$)	E^{ox}_{onset} [b] (V)	E_{gap} [c] (eV)	E_{HOMO}/E_{LUMO} (eV)	μ ($cm^2V^{-1}s^{-1}$)	V_{th} (V)	I_{on}/I_{off} (A/A)
1	263 (32314), 294 (29722)	1.20	3.51	-6.40/-2.89	-	-	-
2	303 (76660)	0.84	3.33	-6.04/-2.71	2×10^{-5}	-16.0	~ 10^1
3	283 (52268), 340 (67146)	0.68	3.57	-5.88/-2.31	7×10^{-3} [e] (1×10^{-3})	-9.6 [e] (-5.5)	~ 10^4
4	317 (79023)	-	3.24	-5.69 [d] /-2.45	3×10^{-2} [f] (1×10^{-2})	-12.8 [f] (-9.0)	~ 10^3

[a] Wavelength of maximum absorption and molar extinction coefficient. [b] Onset oxidation potential. [c] Energy difference between HOMO and LUMO orbitals. [d] Reference 6b. [e] Maximum value registered the 8th day. [f] Maximum value registered the 5th day. The results in parentheses are for measurements after five months in air atmosphere.

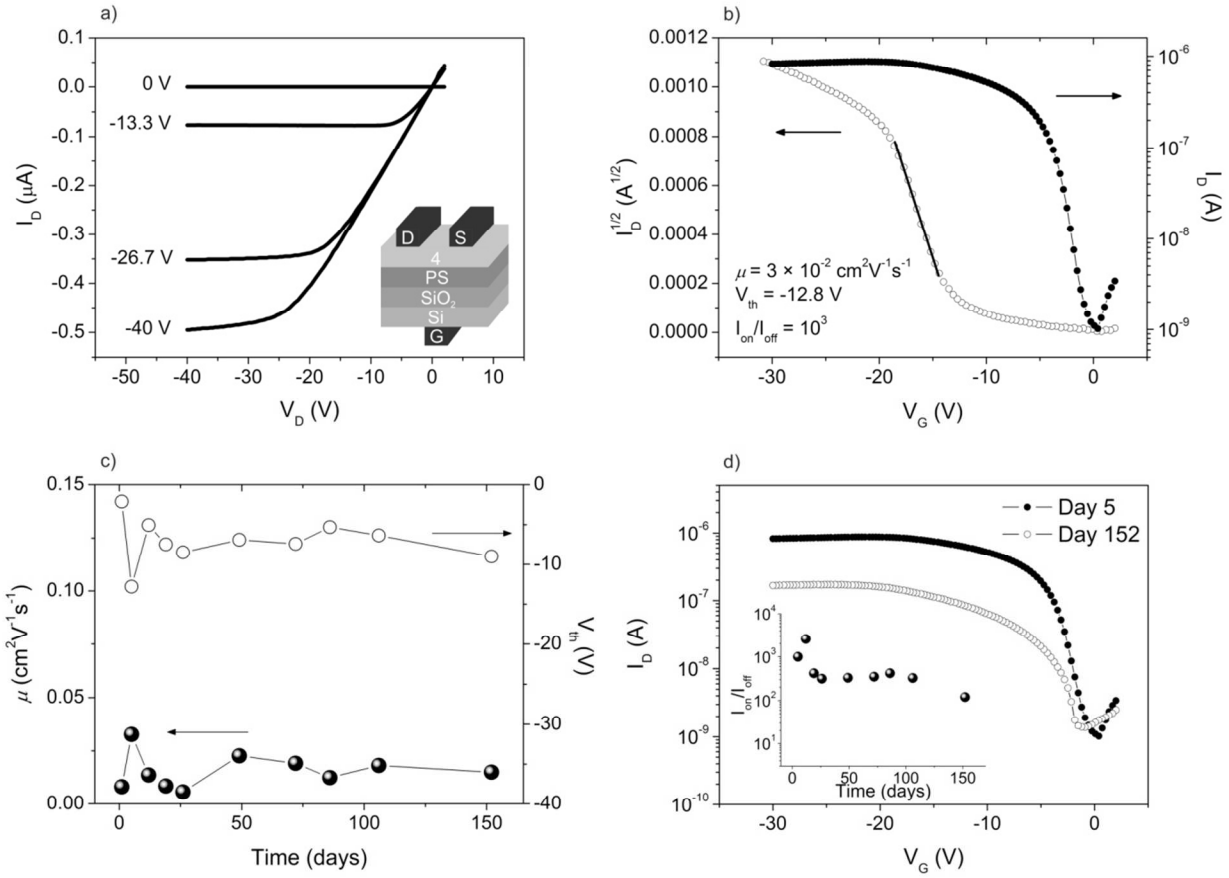

Fig. 3 OTFTs characteristics of device fabricated with **4** as the semiconductor layer and with PS treated substrate. a) Output characteristics at different gate voltages (V_G). b) Transfer (V_D = -20 V) and saturation characteristics. c) Mobility and threshold voltage of one representative device fabricated with **4** as the semiconductor layer and with PS treated substrate as a function of storage time in the air. d) Transfer characteristics for the 5th day and the 152nd day of the experiment at V_D = -20 V. Inset figure shows the evolution with time of the I_{on}/I_{off} ratio of the selected device.

Table 1 collects the device characterization for OTFTs fabricated with the more extended π-conjugated cores of compounds **3** and **4**. Devices fabricated with substrates of 50 nm of SiO_2 presented similar hole mobilities, but lower threshold voltages, than those fabricated from substrates of 110 nm of SiO_2. Reproducibility of the measurements and yield of the working devices were found to be independent of the thickness of the SiO_2 layer. The highest values of charge mobilities were achieved modifying the dielectric surface with a polystyrene thin film layer, which also resulted in lower threshold voltages and higher reproducibility. **3** and **4** PS-treated SiO_2 devices presented a superior yield given by the average of ten devices (**3:** 89% and **4:** 100%) exhibiting all of the tested devices similar performances. The highest hole mobility was registered for triindole **4**, 3 × 10^{-2} $cm^2V^{-1}s^{-1}$ in front of 7 × 10^{-3} $cm^2V^{-1}s^{-1}$ for the indolocarbazole **3**. OTFTs characteristics of **3** and **4** based devices fabricated on bare SiO_2 surfaces showed lower reproducibility and lower charge mobilities of 7 × 10^{-5} and 5 × 10^{-3} $cm^2V^{-1}s^{-1}$, respectively.

A representative output, transfer and saturation characteristics for **4** based OTFTs are shown in figure 3 (Figure 3a-b) for **4** based OTFTs (for OTFTs characteristics of compound **3** based devices see ESI, Fig. S3a-b†). The output characteristics are indicative of the OTFT behaviour of the device in both linear and saturated regions. The hole mobility (μ) in the saturated region and the threshold voltage (V_{th}) were calculated from equation (1):

$$I_D = \frac{WC_{ox}\mu}{2L}(V_G - V_{th})^2 \quad (1)$$

where W and L are the channel width and length, respectively, C_{ox} is the unit dimensional dielectric capacitance of gate insulator, μ is the hole mobility and V_{th} is the threshold voltage.

A key requirement in the design of new semiconductors is the stability under ambient conditions. OTFTs fabricated with both types of semiconductors **3** and **4** operate well in air, exhibiting remarkable ambient storage stability. Similar threshold voltages, mobilities and I_{on}/I_{off} ratios were obtained after 5 months of storage in air and in dark conditions, demonstrating excellent air stability (Figure 3c-d, air-stability experiments for **3** based devices can be found in the ESI, Fig. S3c-d†). The increase in charge mobilities after the first days of exposure to air can be attributed to p-doping of the device by O_2.

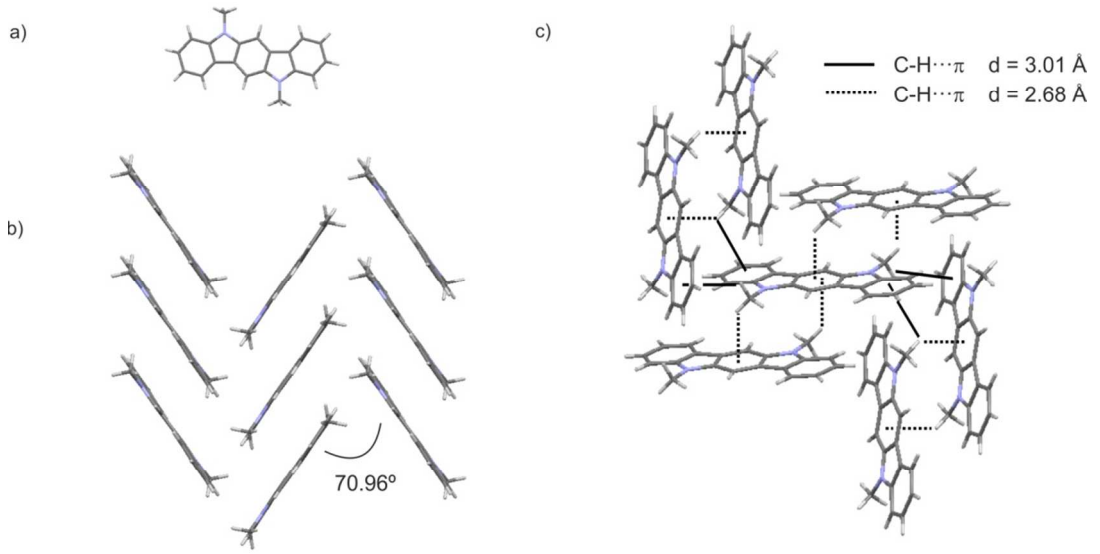

Fig. 4 Single crystal structure of compound **3**. a) Molecular structure, b) herringbone packing motif with its corresponding herringbone angle and c) short contacts given by C-H···π interactions.

Molecular order and morphology of the thin films

For further exploration of the relationship between the OTFTs performance and the role of the molecular order in the thin films, Grazing Incidence X-ray Diffraction (GIXRD) and Atomic Force Microscopy (AFM) analysis were performed.

First of all, the knowledge of the single crystal structure of compounds **3** and **4** was crucial since it could provide the molecular packing motif and main intermolecular interactions of these compounds. The crystal structure of triindole derivative **4** was previously reported[12] to adopt a face-to-face packing in an alternate arrangement due to π-π interactions between adjacent triindole molecules. For that compound two different distances (3.53 Å and 3.68 Å) between two neighbouring molecules were observed due to the steric hindrance induced by the methyl groups.

In order to examine the molecular packing and the intermolecular interactions in indolocarbazole derivative **3**, the single crystal structure was determined by X-ray crystallography. The compound crystallizes in space group C2/c of the monoclinic system with unit-cell dimensions of a = 16.8377(13) Å, b = 5.6889(4) Å, c = 15.3882(11) Å, β = 106.671(2)°, volume = 1412.05(18) Å^3. The cif file and the detailed crystallographic data are provided in the ESI (Table S1-S5† and Fig. S4†).

The X-ray structure of **3** is shown in Figure 4. The molecular structure of indolocarbazole **3** is nearly planar with a small torsion angle around 1.5º (Figure 4a). Molecules exhibit a herringbone packing motif with a herringbone angle of 70.96º (Figure 4b). Every molecule is surrounded by six molecules showing C-H···π interactions between one of the hydrogen atoms of the methyl groups with the central benzene ring of an adjacent indolocarbazole molecule with a distance of 2.68 Å. Moreover, one of the hydrogen atoms of the methyl groups also interacts with one peripheral benzene ring with a distance of 3.01 Å, being responsible for the above-mentioned herringbone packing motif (Figure 4c).

For indolo[3,2-*b*]carbazole derivatives, the packing motif in the solid state strongly depends on the length of the alkyl chain in the nitrogen position of the indolocarbazole derivatives. Different packing motifs have been described in the literature from the non-substituted indolo[3,2-*b*]carbazole[13] to alkylated derivatives.[13,14]

For GIXRD studies, 75-nm thick films were deposited by sublimation in a vacuum system of compounds **3** and **4** on both bare and on polystyrene treated c-Si/SiO_2 surfaces. All thin films showed strong diffraction peaks, which suggested that both **3** and **4** produced well-ordered films under the experimental conditions (Figure 5). As shown in Figure 5a, vacuum deposited **3** thin films on bare and on PS-treated c-Si/SiO_2 surfaces presented identical X-ray diffraction patterns, which means that molecules are equally oriented, both on bare and on PS-treated SiO_2 surfaces. The combination of the GIXRD studies with the powder XRD data and the single crystal structures provides valuable information about the molecular order in the thin films.[13,15]

Thin films based on indolocarbazole **3** presented only one strong diffraction peak in the GIXRD patterns at 2θ = 11.1º, in comparison to the more complex diffractogram spectra obtained from the powder XRD data (Fig. S5a† in the ESI). From the single crystal data and the powder XRD pattern the diffraction peak at 2θ = 11.1º can be undoubtedly assigned to the crystalline plane (200). The GIXRD study shows that the plane (200) is parallel to the c-Si/SiO_2 substrate, i.e. with *b*- and *c*-axis also in the parallel plane. The molecular packing within the thin film corresponds to that of indolocarbazole **3** in the single crystal. This suggests that molecules are located nearly perpendicular, with an angle of 79º, to the substrate (Figure 5a-b).

For vacuum deposited **4** thin films on PS-treated substrates one diffraction peak was mainly observed in the thin film XRD pattern at 2θ = 8.3º together with a second order diffraction peak at 2θ = 16.6º, which is indicative of a higher crystalline thin film than that obtained for indolocarbazole **3**. From the single crystal data[12], the powder XRD pattern (Fig. S5b† in the ESI) and the

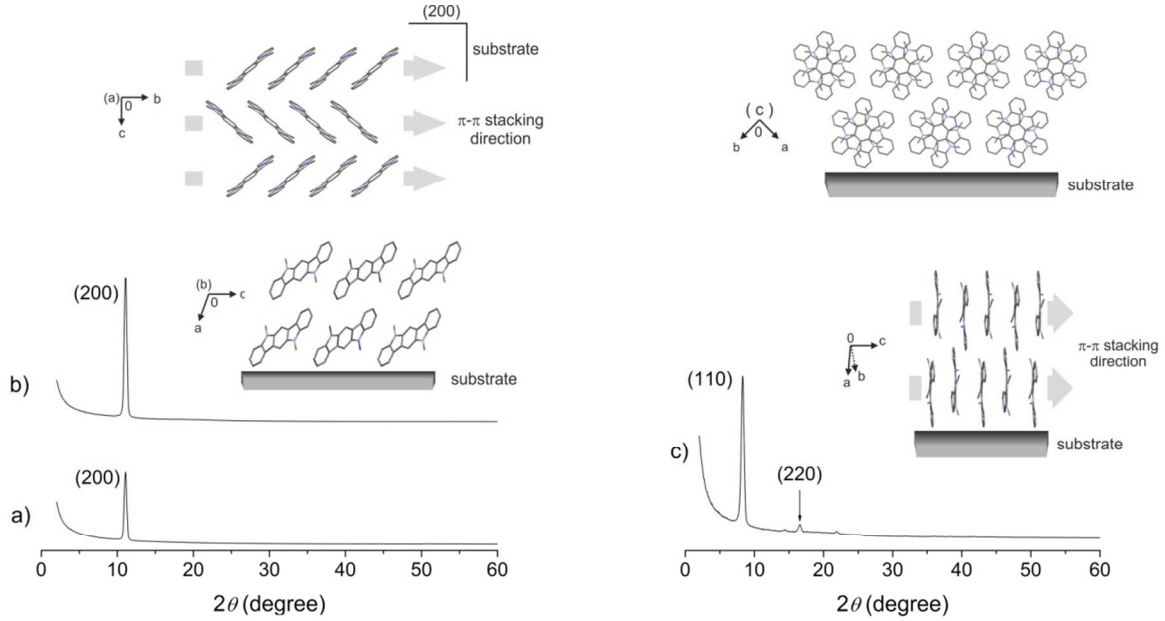

Fig. 5 GIXRD pattern of vacuum-deposited **3** films on a) bare and b) polystyrene treated c-Si/SiO_2 surfaces. The inset image shows the molecular packing of compound **3** with the (200) plane situated parallel to the paper (above) and perpendicular to the paper (below). c) GIXRD pattern of vacuum-deposited **4** film on polystyrene treated c-Si/SiO_2 surface. The inset images show the molecular packing in the thin films seen from two different perspectives, being the (110) plane situated perpendicular to the paper. The hydrogen atoms were omitted for clarity.

GIXRD data, the diffraction peaks at 2θ = 8.3º and 2θ = 16.6º were assigned to the corresponding planes (110) and (220), respectively. Therefore, in the GIXRD pattern the (hk0) planes are mainly observed, suggesting that these planes are parallel to the substrate with the *c*-axis also in the parallel plane. Consequently, as it is collected in Figure 5c, triindole molecules are located totally perpendicular (90º) to the substrate surface.

In the OTFTs performance the best charge carrier mobility was found for the triindole derivative **4** based devices in comparison with those obtained from the indolocarbazole **3**. This improvement in the charge carrier mobility value can be related with the different packing motifs and the corresponding different intermolecular interactions, and with different molecular order into the thin films. From the single crystal data reported above, it can be established that a change in the packing motif exists from the herringbone of compound **3** with $CH_3\cdots\pi$ interactions to a face-to-face arrangement of compound **4** dominated by π-π interactions, where the electronic coupling is maximized and the charge transport should be favoured. As a second important point, GIXRD suggests that molecules in **4** are located completely perpendicular to the substrate, which seems to be the best molecular disposition for the charge transport through the semiconductor active layer of an OTFT with bottom gate - top contact geometry.

In addition to the local intermolecular interactions, the film morphology and the grain sizes and boundaries strongly influence the charge transport properties, particularly at the interface between the semiconductor and the dielectric. AFM images were taken from **3** and **4** films deposited by sublimation on both bare and polystyrene treated SiO_2 surfaces (Figure 6). Remarkable morphology differences were observed between them.

Thin films based on indolocarbazole **3** deposited on bare SiO_2 and on PS-treated surfaces showed similar topography profiles. Both films present a similar average grain size, with average

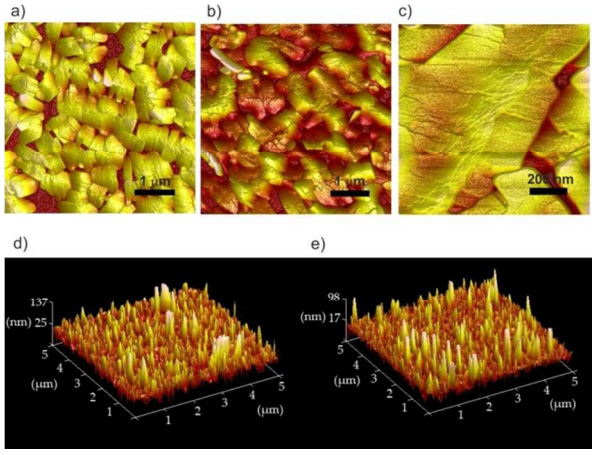

Fig. 6 AFM images of vacuum-deposited **3** films deposited on a) bare SiO_2 (5 × 5 μm^2), b) polystyrene treated SiO_2 (5 × 5 μm^2) and c) polystyrene treated SiO_2 (1 × 1 μm^2). AFM images of vacuum-deposited **4** films deposited on d) bare SiO_2 (5 × 5 μm^2) and e) polystyrene treated SiO_2 (5 × 5 μm^2).

width of 600 nm and lengths that include from 600 to 1400 nm. Only an slightly enhancement of the interconnectivity between grains is observed for films based on **3** deposited on PS-treated surfaces, which actually correspond to a higher device performance (Figure 6a-b, Table 1). Vacuum-deposited **3** films presented a terrace-like step morphology (Figure 6c), independently of the modification of the dielectric surface.

Vacuum-deposited **4** films on bare and on PS-treated SiO_2 also presented identical morphologies independently of the modification of the dielectric surface (Figure 6d-e). AFM images exhibited protrusions/hillocks whose average thickness was in the order of 130 nm and their height varies from 50 to more than 100 nm.

Combining GIXRD and AFM data, it can be established that vacuum deposited films of indolocarbazole **3** and triindole **4** derivatives, respectively, on bare and on PS-treated SiO_2 surfaces presented identical X-ray diffraction patterns and morphology. Therefore, the addition of a polystyrene SAM has a null influence in the growth of the molecular order and on the morphology of the thin film. The improvement of the electrical characteristics of the OTFT devices observed in PS-treated c-Si/SiO_2 substrates seems then to be related to the improvement of the interface contact between the dielectric and the semiconductor layer.

Experimental section

Materials

All reagents for synthesis were obtained from commercial sources and were used as received without further purification. Indolo[3,2-*b*]carbazole was synthesized according to the literature.[10] Triazatruxene was synthesized according to the reported method.[11]

Synthesis of 9,9'-dimethyl-9*H*,9*H*'-[3,3']bicarbazole (2)

9-methyl-9*H*-carbazole **1** (3.8 g, 31.1 mmol) was dissolved in anhydrous $CHCl_3$ (70 mL) under inert atmosphere. After, $FeCl_3$ (13.7 g, 84.5 mmol) was added and the reaction mixture was stirred at room temperature for 30 minutes. Then, the mixture was poured into methanol and the formation of a precipitate was observed. The solid was isolated by vacuum filtration, washed thoroughly with methanol and dried. The crude was purified by flash column chromatography using a mixture of hexane and CH_2Cl_2 (1:1 v/v) as eluent to give compound **2** (4.3 g, 73%). ^{1}H NMR (400 MHz, d_6-DMSO), δ: 8.55 (d, J = 1.7 Hz, 2H), 8.26 (d, J = 8.3 Hz, 2H), 7.89 (dd, J = 8.5 Hz, J = 1.7 Hz, 2H), 7.67 (d, J = 8.5 Hz, 2H), 7.58 (d, J = 8.2 Hz, 2H), 7.50-7.46 (m, 2H), 7.24-7.21 (m, 2H), 3.92 (s, 6H, N-CH_3) ppm. ^{13}C NMR (100 MHz, d_6-DMSO), δ: 141.1, 139.7, 132.2, 125.8, 125.0, 122.7, 122.3, 120.4, 118.7, 118.2, 109.4, 109.2, 29.1 ppm. HRMS (ESI-MS) (*m/z*): calcd for $C_{26}H_{21}N_2$ $(M+H)^+$ 361.1699, found: 361.1684.

Synthesis of 5,11-dimethyl-indolo[3,2-*b*]carbazole (3)

NaH (12 mg, 0.52 mmol) was added to a solution of indolo[3,2-*b*]carbazole (60 mg, 0.23 mmol) in anhydrous DMF under inert atmosphere. The solution was stirred at room temperature for 30 minutes. Then, methyl iodide (32 µL, 0.52 mmol) was added and the mixture was stirred at room temperature for 30 minutes and then treated with H_2O. The aqueous layer was extracted with dichloromethane and the organic layer was dried over Na_2SO_4. The solvent was removed by evaporation and the crude was purified by flash column chromatography using a mixture of hexane and dichloromethane (4:1 v/v) to give compound **3** (55 mg, 83%).^{1}H NMR (400 MHz, $CDCl_3$), δ: 8.20 (d, J = 8.0 Hz, 2H), 8.02 (s, 2H), 7.53-7.49 (m, 2H), 7.42 (d, J = 8.0 Hz, 2H), 7.26-7.22 (m, 2H), 3.96 (s, 6H, N-CH_3) ppm. ^{13}C NMR (100 MHz, $CDCl_3$), δ = 142.3, 136.9, 125.8, 123.0, 122.9, 120.3, 118.2, 108.3, 98.7, 29.5 ppm. HRMS (ESI-MS) (*m/z*): calcd for $C_{20}H_{17}N_2$ $(M+H)^+$ 285.1386, found: 285.1382.

Synthesis of *N*-trimethyltriindole (4)

NaH (98 mg, 4.05 mmol) was added to a solution of triazatruxene (0.28 g, 0.81 mmol) in anhydrous DMF under inert atmosphere. The solution was stirred at room temperature for 30 minutes. Then, methyl iodide (166 µL, 2.67 mmol) was added and the mixture was stirred at room temperature for 30 minutes and then treated with H_2O. The aqueous layer was extracted with dichloromethane and the organic layer was dried over Na_2SO_4. The solvent was removed by evaporation and the crude was purified by flash column chromatography using a mixture of hexane and dichloromethane (5:1 v/v) as eluent to give compound **4** (0.26 g, 84%). ^{1}H NMR (400 MHz, $CDCl_3$), δ: 8.47 (d, J = 8.0 Hz, 3H), 7.59 (d, J = 8.0 Hz, 3H), 7.49-7.45 (m, 3H), 7.37-7.33 (m, 3H), 4.48 (s, 9H, N-CH_3) ppm. ^{13}C NMR (100 MHz, $CDCl_3$), δ = 142.1, 139.2, 123.0 (2C), 121.9, 120.0, 109.8, 102.7, 36.1 ppm. HRMS (ESI-MS) (*m/z*): calcd for $C_{27}H_{22}N_3$ $(M+H)^+$ 388.1808, found: 388.1810.

Instrumentation and methods

Flash column chromatography was carried out over silica gel (SDS, 230-240 mesh). ^{1}H NMR (400 MHz) and ^{13}C NMR (100 MHz) spectra were collected on a Varian Mercury spectrophotometer. NMR spectra have been processed with the MestRec Nova software. HRMS was performed in a LC/MSD-TOF Agilent Technologies apparatus by means of the electrospray (ESI-MS) technique. UV-Vis spectra were registered in a Varian Cary UV-Vis-NIR 500E spectrophotometer. TGA were performed with a Mettler Toledo TGA/SDTA 851e instrument at a heating rate of 10 K min^{-1}. Differential scanning calorimetry (DSC) thermograms were recorded using a Mettler-Toledo DSC821 module under nitrogen flow. Cyclic voltammograms were carried out in a microcomputer-controlled potentiostat/galvanostat Autolab with PGSTAT30 equipment and GPES software. A cylindrical three-electrode cell was used. The reference electrode was a Metrohm Ag/AgCl/KCl (3M) mounted in a Luggin capillary containing a 0.1 M solution of tetrabutylammonium perchlorate (TBAP) in dichloromethane. The counter and working electrodes were a platinum spiral and a platinum wire, respectively. All voltammetric curves were recorded under quiescent conditions, at a scan rate of 100 mV s^{-1} and under argon atmosphere. All solutions were prepared in dichloromethane (1 mM). Tetrabutylammonium perchlorate (Aldrich, electrochemical grade) was used as a supporting electrolyte. The energy of the HOMO level was estimated from the onset of the first oxidation peak as E_{HOMO} = -E_{onset}^{ox} +

$E^0(Fc/Fc^+)$ – 5.39 where $E^0(Fc/Fc^+)$ = +0.19 V *vs*. Ag/AgCl/KCl (3M) and -5.39 eV corresponds to the formal potential of the Fc^+/Fc redox couple in the Fermi scale.[16] The energy of the LUMO level was calculated as $E_{LUMO} = E_{HOMO} + E_{gap}$. Single-crystal analysis of material **3** was performed on a D8 Venture system equipped with a multilayer monochromator and a Mo high brilliance Incoatec Microfocus Source (λ = 0.71073 Å). The frames were integrated with the Bruker SAINT software package using a narrow-frame algorithm. The structure was solved and refined using the Bruker SHELXTL Software Package. Powder X-ray diffraction (XRD) measurements were obtained by using a PANalytical X'Pert PRO MPD θ/θ powder diffractometer, in a configuration of convergent beam with a focalizing mirror and transmission geometry with a spinner glass capillary sample holder, a PIXcel detector and with Cu Kα radiation at 45 kV and 40 mA. Samples were prepared by introduction of powder materials **3** and **4** in *Lindemann* glass capillaries of 0.5 millimetres of diameter. Grazing incidence XRD (GIXRD) measurements of the thin-films of the sublimated organic materials were performed in a PANalytical X'Pert PRO MRD diffractometer with a PIXcel detector, a parabolic Göbel mirror at the incident beam and a parallel plate collimator at the diffracted beam, and with Cu Kα radiation at 45 kV and 40 mA. The angle of incidence used was ω = 0.17°. Thin films (75 nm) were prepared from compounds **3** and **4** by sublimation on a vacuum system on a c-Si/SiO_2 substrate and on polystyrene-treated c-Si/SiO_2 substrates with the deposition rate at 0.3 Å s^{-1} under a pressure below 10^{-6} mbar. AFM experiments were conducted using a AFM Dimension 3100 system attached to a Nanoscope IVa electronics unit (Bruker).

OTFT device fabrication

OTFTs devices were fabricated using the bottom gate - top contact geometry. The substrate consisted in a thermally oxidized crystalline silicon wafer that provided the gate dielectric (SiO_2) of thickness 50 nm and 110 nm. Polystyrene (PS) was used as a self-assembled monolayer to improve the device performance. A solution of PS in toluene (4 mg/mL) was deposited dropwise on the substrate. The substrate was spun at 500 rpm for 5 s and 2500 rpm for 30 s with a P6700 spin coater. Organic materials **2**-**4** were deposited by sublimation in a vacuum system with base pressure below 10^{-6} mbar. The sublimation temperature for the organic compounds was regulated from 152 to 160ºC, 120 to 130ºC and 160 to 170ºC, respectively, to maintain a stable deposition rate around 0.3 Å s^{-1} to obtain a 75 nm thickness layer. Then, they were transferred to a different vacuum chamber used to evaporate the metallic contacts. Gold was used as source and drain electrodes, which were defined using a metallic mask that defines a channel length (L) and width (W) of 80 μm and 2 mm, respectively. The fabricated OTFTs were electrically characterized in dark and under air conditions. The electrical characteristics were measured using an Agilent 4156C parameter analyser.

Conclusions

All carbazole-based compounds **1**-**4** presented low HOMO levels and high HOMO-LUMO gaps indicating their potential hole transporting properties and air-stability. However, only compounds **3** and **4**, with extended π-conjugated cores with two and three fused carbazole rings, presented good device performances and air-stability and durability under air conditions, for longer periods up to 5 months, with hole mobility values ranging from 10^{-3} to 10^{-2} cm^2 V^{-1} s^{-1}. For indolocarbazole derivative **3**, a herringbone packing motif with $CH_3\cdots\pi$ interactions has been described in the semiconductor layer, whereas a cofacial molecular packing is observed for triindole **4**. For the latter, it has been found that in the crystal structure and in the thin film, presents a face-to-face molecular packing, exhibiting the best OTFT performance. For this material an optimal perpendicular molecular disposition to the substrate surface has been determined by GIXRD. Indolo[3,2-*b*]carbazole and specially triindole units are promising π-conjugated cores for new organic semiconductors for electronic devices.

Notes and references

[a] *Grup de Materials Orgànics, Institut de Nanociència i Nanotecnologia (IN²UB), Departament de Química Orgànica, Universitat de Barcelona, Martí i Franquès 1, E-08028, Barcelona, Spain. Fax: +34 93 339 78 78; Tel: +34 93 403 92 60; E-mail: dvelasco@ub.edu*

[b] *Dept. Eng. Electrònica & Centre de Recerca en Nanoenginyeria, Universitat Politècnica de Catalunya, C/ Jordi Girona, 1-3, 08034, Barcelona, Spain. Tel: +34 93 401 10 02; E-mail: joaquim.puigdollers@upc.edu*

† Electronic Supplementary Information (ESI) available: [Absorption spectra, cyclic voltammograms, OTFTs characteristics, detailed crystallographic data and powder X-ray diffraction patterns]. See DOI: 10.1039/b000000x/

1 a) R. Fitzner, E. Mena-Osteritz, A. Mishra, G. Schulz, E. Reinold, M. Weil, C. Körner, H. Ziehlke, C. Elschner, K. Leo, M. Riede, M. Pfeiffer, C. Uhrich, P. Bäuerle, *J. Am. Chem. Soc.*, 2012, **134**, 11064. b) J. Mei, Y. Diao, A. L. Appleton, L. Fang, Z. Bao, *J. Am. Chem. Soc.*, 2013, **135**, 6724.

2 a) M. E. Roberts, S. C. B. Mannsfeld, N. Queraltó, C. Reese, J. Locklin, W. Knoll, Z. Bao, *PNAS*, 2008, **105**(34), 12134. b) H. Klauk, M. Halik, U. Zschieschang, G. Schmid, W. Radlik, W. Weber, *J. Appl. Phys.,* 2002, **92**, 5259.

3 a) D. Simeone, S. Cipolloni, L. Mariucci, M. Rapisarda, A. Minotti, A. Pecora, M. Cuscunà, L. Maiolo, G. Fortunato, *Thin Solid Films,* 2009, **517**, 6283.b) K. Takimiya, T. Yamamoto, H. Ebata, T. Izawa, *Science and Technology of Advanced Materials*, 2007, **8**, 273.

4 a) S. Castellanos, V. Gaidelis, V. Jankauskas, J. Grazulevicius, E. Brillas, F. López-Calahorra, L. Juliá, D. Velasco, *Chem. Commun*., 2010, **46**, 5130. b) A. Tomkeviciene, J. V. Grazulevicius, D. Volyniuk, V. Jankauskas, G. Sini, *Phys. Chem. Chem. Phys*, 2014, **16**, 13932. c) Y. M. Tao, H. Y. Li, Q. L. Xu, Y. C. Zhu, L. C. Kang, Y. X. Zheng, J.-L. Zuo, X. Z. You, *Synth. Met.*, 2011, **161**, 718. d) J.-F. Morin, M. Leclerc, D. Adès, A. Siove, *Macromol. Rapid. Commun*., 2005, **26**, 761.

5 a) H. Zhao, L. Jiang, H. Dong, H. Li, W. Hu, B. S. Ong. *Chem. Phys. Chem*., 2009, **10**, 2345. b) P.-L. T. Boudreault, S. Wakim, M. L. Tang, Y. Tao, Z. Bao, M. Leclerc, *J. Mater. Chem.,* 2009, **19**, 2921.

6 a) X. Qian, Y.-Z. Zhu, J. Song, X.-P. Gao, J.-Y. Zheng, *Org. Lett.,* 2013, **15**(23), 6034. b) S. W. Shelton, T. L. Chen, D. E. Barclay, B. Ma, *Appl. Mater. Interfaces,* 2012, **4**, 2534.

7 a) D. H. Hug, G. W. Kim, G. H. Kim, C. Kulshreshta, J. H. Kwon, *Synthetic Metals*, 2013, **180**, 79. b) W. Y. Lai, Q. Y. He, R. Zhu, Q. Q. Chen, W. Huang, *Adv. Funct. Mater.,* 2008, **18**, 265.

8 E. M. García-Frutos, U. K. Pandey, R. Termine, A. Omenat, J. Barberá, J. L. Serrano, A. Golemme, B. Gómez-Lor, *Angew. Chem. Int. Ed.,* 2011, **50**, 7399.

9 a) V. Vaitkeviciene, S. Grigalevicius, J. V. Grazulevicius, V. Jankauskas, V. G. Syromyatnikov, *European Polymer Journal,* 2006, **42**, 2254. b) T. Tokuda, K. Murashiro, M. Kubo, H. Masu, M.

Imanari, H. Seki, N. Aoki, Y. Ochiai, H. Kanoh, K. Hoshino, *Langmuir*, 2012, **28**, 16430.
10 B. Robinson, *J. Chem. Soc.,* 1963, 3097.
11 a) M. Franceschin, L. Ginnari-Satriani, A. Alvino, G. Ortaggi, A. Bianco, *Eur. J. Org. Chem.,* 2010, **1**, 134. b) L. Ji, Q. Fang, M.-S. Yuan, Z.-Q. Liu, Y.-X. Shen, H.-F. Chen, *Org. Lett.,* 2010, **12**(22), 5192.
12 M. García-Frutos, E. Gutierrez-Puebla, M. A. Monge, R. Ramírez, P. de Andrés, A. de Andrés, R. Ramírez, B. Gómez-Lor, *Organic Electronics,* 2009, **10**, 643.
13 G. Zhao, H. Dong, H. Zhao, L. Jiang, X. Zhang, J. Tan, Q. Meng, W. Hu, *J. Mater. Chem.,* 2012, **22**, 4409.
14 S. Wakim, J. Bouchard, M. Simard, N. Drolet, Y. Tao, M. Leclerc, *Chem. Mater.,* 2004, **16**, 4386.
15 15 P.-L. T. Boudreault, S. Wakim, N. Blouin, M. Simard, C. Tessier, Y. Tao, M. Leclerc. *J. Am. Chem. Soc*., 2007, **129**, 9125.
16 a) C. M. Cardona, W. Li, A. E. Kaifer, D. Stockdale, G. C. Bazan, *Adv. Mater.*, 2011, **23**, 2367. b) A. J. Bard, L. R. Faulkner, *Electrochemical Methods: Fundamentals and Applications*, WILEY-VCH, New York, **2001**.

Acknowledgements

Financial support from the *Ministerio de Economía y Competitividad* (CTQ2012-36074 and TEC2011-27859) is gratefully acknowledged. M. Reig grates for the grant ADR from *Universitat de Barcelona* (UB). We also thank Xavier Alcobé and Josep Mª Bassas from the X-ray diffraction unit of the Scientific and Technological Centers of the University of Barcelona (CCiTUB) for the realization of the X-ray diffraction measurements and their helpful discussion.

GRAPHICAL ABSTRACT

Correlation of the OTFT performance with the molecular order in the semiconductor layers in function of the extension of the π-conjugated core of a series of carbazole based organic semiconductors.

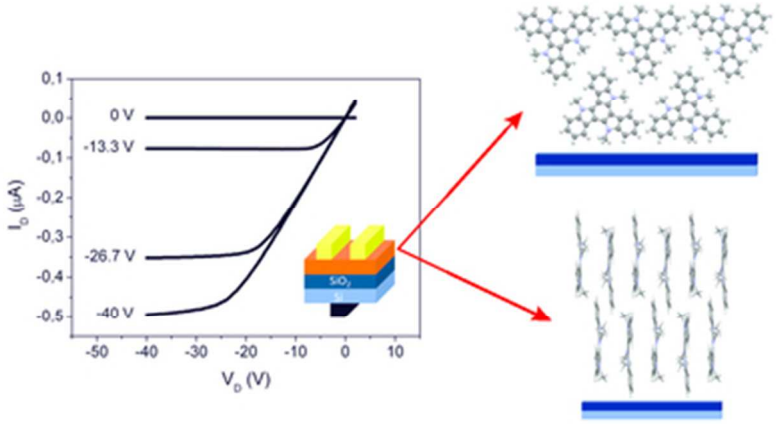

33x18mm (300 x 300 DPI)